Multiple Interferon Regulatory Factor and NF- κB Sites Cooperate in Mediating Cell-Type- and Maturation-Specific Activation of the Human *CD83* Promoter in Dendritic Cells

Marcello F. Stein, Stefan Lang, Thomas H. Winkler, Andrea Deinzer, Sebastian Erber, Dirk M. Nettelbeck, Elisabeth Naschberger, Ramona Jochmann, Michael Stürzl, Robert K. Slany, Thomas Werner, Alexander Steinkasserer and Ilka Knippertz

Updated information and services can be found at:
http://mcb.asm.org/content/33/7/1331

These include:

SUPPLEMENTAL MATERIAL

Supplemental material

REFERENCES

This article cites 55 articles, 20 of which can be accessed free
at: http://mcb.asm.org/content/33/7/1331#ref-list-1

CONTENT ALERTS

Receive: RSS Feeds, eTOCs, free email alerts (when new
articles cite this article), more»

Multiple Interferon Regulatory Factor and NF-κB Sites Cooperate in Mediating Cell-Type- and Maturation-Specific Activation of the Human *CD83* Promoter in Dendritic Cells

Marcello F. Stein,[a] Stefan Lang,[b*] Thomas H. Winkler,[b] Andrea Deinzer,[a] Sebastian Erber,[a] Dirk M. Nettelbeck,[c] Elisabeth Naschberger,[d] Ramona Jochmann,[d] Michael Stürzl,[d] Robert K. Slany,[e] Thomas Werner,[f,g] Alexander Steinkasserer,[a] Ilka Knippertz[a]

Department of Immune Modulation at the Department of Dermatology, University Hospital Erlangen, Erlangen, Germany[a]; Department of Biology, Nikolaus-Fiebiger Center for Molecular Medicine, Friedrich-Alexander University Erlangen-Nuremberg, Erlangen, Germany[b]; Helmholtz University Group Oncolytic Adenoviruses at the DKFZ (German Cancer Research Center) and Department of Dermatology, Heidelberg University Hospital, Heidelberg, Germany[c]; Division of Molecular and Experimental Surgery, Department of Surgery, University Medical Center Erlangen, Erlangen, Germany[d]; Department of Genetics, University Erlangen, Erlangen, Germany[e]; Genomatix Software GmbH, Munich, Germany[f]; Internal Medicine, Nephrology, University of Michigan, Ann Arbor, Michigan, USA[g]

CD83 is one of the best-known surface markers for fully mature dendritic cells (mature DCs), and its cell-type- and maturation-specific regulation makes the CD83 promoter an interesting tool for the genetic modulation of DCs. To determine the mechanisms regulating this DC- and maturation-specific CD83 expression, chromatin immunoprecipitation (ChIP)-on-chip microarray, biocomputational, reporter, electrophoretic mobility shift assay (EMSA), and ChIP analyses were performed. These studies led to the identification of a ternary transcriptional activation complex composed of an upstream regulatory element, a minimal promoter, and an enhancer, which have not been reported in this arrangement for any other gene so far. Notably, these DNA regions contain a complex framework of interferon regulatory factor (IRF)- and NF-κB transcription factor-binding sites mediating their arrangement. Mutation of any of the IRF-binding sites resulted in a significant loss of promoter activity, whereas overexpression of NF-κB transcription factors clearly enhanced transcription. We identified IRF-1, IRF-2, IRF-5, p50, p65, and cRel to be involved in regulating maturation-specific CD83 expression in DCs. Therefore, the characterization of this promoter complex not only contributes to the knowledge of DC-specific gene regulation but also suggests the involvement of a transcriptional module with binding sites separated into distinct regions in transcriptional activation as well as cell-type- and maturation-specific transcriptional targeting of DCs.

Dendritic cells (DCs) are the most important antigen-presenting cells (APCs), since only DCs are able to induce naive immune responses (1). In order to induce potent immune responses, DCs have to mature. One of the most prominently up-regulated molecules during this maturation process is CD83 (2). Two naturally occurring CD83 isoforms have been described, a membrane-bound form (mCD83) and a soluble form (sCD83), which is generated by a proteolytic cleavage of the extracellular domain of mCD83 (3). However, both are derived from the same transcript. It has been shown that mCD83 expressed on mature DCs (mDCs) has immunostimulatory properties. Blockade of the CD83 mRNA export from the nucleus into the cytoplasm and thereby inhibition of cell surface expression led to strongly reduced DC-mediated T cell stimulation (4). Further evidence for the functional importance of mCD83 was derived from studies where DCs were electroporated with small interfering RNA (siRNA) to specifically inhibit CD83 expression. These DCs showed a strongly reduced T cell-stimulatory capacity, were unable to prime tumor-specific T lymphocytes, and revealed strongly reduced cytokine expression profiles (5, 6). On the other hand, overexpression of mCD83 on DCs led to enhanced T cell stimulation (5, 7). Thus, these data clearly indicate that mCD83 expressed on mature DCs acts as a costimulatory molecule and is essential for DC-mediated T cell stimulation.

Soluble CD83, on the other hand, has immunosuppressive activities, thereby downmodulating immune responses. In this respect, it has been shown that sCD83 blocks DC-mediated T cell

stimulation *in vitro* (8, 9). *In vivo* studies revealed that sCD83 also has a very interesting therapeutic potential, inhibiting, for instance, paralysis very efficiently in the experimental autoimmune encephalomyelitis (EAE) model (10). In organ transplantations, it was shown that sCD83 prevents rejection of allogeneic heart and skin as well as kidney transplants in several animal models (11, 12). Thus, sCD83 has a promising immune-modulating capacity. However, the precise biological function and the transcriptional regulation of *CD83* are largely unknown.

A minimal promoter region of 261 bp was reported in 2002 to drive human CD83 expression (13). However, this minimal promoter was neither maturation nor cell type specific, as it showed comparable activities not only in the murine DC-like cell line DC2.4 but also in U937 (human histiocytic lymphoma cell line)

and Jurkat (human leukemic T cell line) cells. Gene expression is controlled by carefully orchestrated processes including chromatin rearrangement, transcriptional regulatory elements, and molecular machinery including activators and transcription factors (TFs) (14). The DNA-binding sites for activators, so-called transcription factor-binding sites (TFBSs), impact the regulatory output and affect the structure of a bound activator, altering its activity (15, 16). TFs in combination with RNA polymerase and associated proteins regulate transcription at the promoter site by forming an unique three-dimensional protein complex. Hence, promoters that act in the same biological context or function in synchronization often display convergence in regard to distance and orientation within their TFBSs (17). To understand the molecular mechanisms regulating cell-type- and activation/maturation-specific gene expression, it is important to determine the transcriptional regulatory elements associated with the gene of interest. Here we report for the first time the characterization of a ternary transcriptional module involving three genomic DNA elements containing interferon regulatory factor (IRF) and NF-κB TFBSs, using techniques including chromatin immunoprecipitation (ChIP)-on-chip microarray, electrophoretic mobility shift assay (EMSA), ChIP, and biocomputational analyses. By a ChIP-on-chip microarray against lysine 9 acetylated histone 3 (H3K9Ac), we identified a highly transcriptionally active region within the CD83 gene locus, particularly in mature DCs. Moreover, the biocomputational analysis revealed a complex framework of NF-κB and IRF TFBSs within these regions. All described elements were shown to be essential for maximal cell-type- and maturation-specific transcriptional activation of the *CD83* gene in mature DCs. They did not mediate this type of specific activation in immature DCs (iDCs), which induce tolerance mechanisms, or in other cells expressing CD83, such as subsets of activated B and T cells. We verified the binding of TFs of the IRF and NF-κB family to the CD83 promoter complex by EMSA as well as ChIP analysis and assessed functionality by cotransfection analyses. NF-κB family members (p50, p65, and cRel) were shown to synergize with interferon regulatory factors, including IRF-1, IRF-2, and IRF-5, in the regulation of human CD83 expression, although NF-κB and IRF TFBSs were located in distinct and separated DNA regions (upstream regulatory element [URE], minimal promoter, and enhancer). These results not only help us to understand the gene regulatory mechanisms linked to DCs and other immune cells but also allow the construction of expression vectors specifically active in mature DCs.

MATERIALS AND METHODS

Generation of human DCs. Human DCs were generated as described previously (18). In short, peripheral blood mononuclear cells (PBMCs) were prepared from leukapheresis products of healthy donors by density centrifugation using Lymphoprep (Axis-Shield PoC), followed by plastic adherence. The nonadherent cell fraction (NAF) was removed for later isolation of CD19$^+$, CD4$^+$, and CD8$^+$ lymphocytes, whereas the adherent cell fraction was cultured for 4 days in medium consisting of RPMI 1640 (Lonza) supplemented with 1% (vol/vol) each heat-inactivated autologous plasma and penicillin–streptomycin–L-glutamine (PAA Laboratories) and 10 mM HEPES (Lonza) as well as 800 IU/ml (day 0) or 400 IU/ml (day 3) recombinant human granulocyte-macrophage colony-stimulating factor (GM-CSF) and 250 IU/ml (days 0 and 3) recombinant interleukin-4 (IL-4) (both from Cell Genix). On day 4, immature DCs (iDCs) were used for further experiments. Maturation of DCs was induced by the

addition of a maturation cocktail (MC) consisting of 200 U/ml IL-1β, 1,000 U/ml IL-6 (both from Cell Genix), 10 ng/ml tumor necrosis factor alpha (TNF-α) (Beromun; Boehringer Ingelheim), and 1 μg/ml prostaglandin E$_2$ (PGE$_2$) (Prostin E$_2$; Pfizer) for 20 h or by the addition of 0.1 ng/ml lipopolysaccharide (LPS) (Sigma) for 3 to 24 h.

Generation of B and T cells. CD19$^+$ B cells and CD4$^+$ and CD8$^+$ T cells were enriched from the NAF by using BD IMag anti-human CD19, CD4, or CD8 particles-DM (all from BD Biosciences) according to the manufacturer's protocol. CD19$^+$ B cells were then cultivated for 5 days at 37°C in 5% CO$_2$ in RPMI 1640 (Lonza) supplemented with 10% (vol/vol) heat-inactivated human serum type AB (Lonza), 1% (vol/vol) penicillin–streptomycin–L-glutamine (PAA Laboratories), 10 mM HEPES (Lonza), and 10 μg/ml pokeweed mitogen (PWM; Sigma) before electroporation. CD4$^+$ and CD8$^+$ T cells were cultured for 2 days at 37°C in 5% CO$_2$ in the medium described above but with 1 μg/ml lectin from *Phaseolus vulgaris* (PHA-P; Sigma) instead of PWM and 10^3 IU/ml IL-2 (Proleukin S; Novartis). Purity of enriched CD19$^+$, CD4$^+$, and CD8$^+$ lymphocytes was assessed by flow cytometric analyses and was revealed to be >98%.

Cells and reagents. Human foreskin fibroblasts (HFF) were cultured in minimum essential medium (MEM; Lonza) supplemented with 7.5% (vol/vol) fetal calf serum (FCS), 1% (vol/vol) glutamine, and 0.001% (vol/vol) gentamicin (all from (PAA Laboratories). NIH 3T3, HeLa, and 293T cells were cultured in Dulbecco's modified Eagle medium (DMEM; Lonza) supplemented with 10% (vol/vol) FCS and 1% (vol/vol) penicillin–streptomycin–L-glutamine (PAA Laboratories), XS52 cells, kindly provided by A. Takashima (University of Texas Southwestern Medical Center, Dallas, TX), were cultured in Iscove's modified Dulbecco's medium (IMDM; Lonza) supplemented with 10% (vol/vol) FCS, 1% (vol/vol) penicillin–streptomycin–L-glutamine, 1% (vol/vol) sodium pyruvate (PAA Laboratories), 10% (vol/vol) NS47 supernatant, and 10 ng/ml murine GM-CSF. 293 (Quantum) cells were cultured in RPMI 1640 (Lonza) supplemented with 10% (vol/vol) FCS and 1% (vol/vol) penicillin–streptomycin–L-glutamine.

Two-step PCR. Two-step PCR was used to amplify the precipitated DNA for hybridization on the ChIP-chip microarray. In the first step, the PCR template was generated by the use of Klenow-Exo$^+$ (NEB). In the second step, the template from the first reaction was amplified with *Taq* polymerase from BioTherm. Both reactions were performed according to the manufacturers' instructions.

Plasmid vectors. The promoterless pGL3/Basic vector (Promega) was used to generate the CD83 promoter complex and control gene reporter constructs by standard cloning procedures. The P-510 sequence was synthesized by GeneArt (Regensburg, Germany) and subsequently cloned into the pGL3/Basic vector (Promega). Mutations of IRF-binding sites were performed by PCR mutagenesis. Coding sequences of p50 (NF-κB1), p65 (RelA), cRel, and IRF-5 were obtained from E. Naschberger (Division of Molecular and Experimental Surgery, Erlangen, Germany [p50, p65, and cRel]) and M. Schmidt (Virology Institute, Erlangen, Germany) and subsequently recloned into the pCDNA3.1 vector (Invitrogen). All plasmids for transient-transfection experiments were purified by standard endotoxin-free anion-exchange columns (Qiagen) and verified by DNA sequencing (MWG Biotech).

Primers. A list of primers used for two-step PCR, cloning, reverse transcription-PCR (RT-PCR), and quantitative PCR (qPCR) is provided in Table S1 in the supplemental material.

Electroporation of DCs and B and T cells. Two million iDCs were electroporated with 4 μg of DNA by using the Human Dendritic Cell Nucleofector kit and an Amaxa Nucleofector I device (both from Lonza) according to the manufacturer's protocol. After electroporation, cells were split into two parts and either matured with 0.1 ng/ml LPS (Sigma) for 20 h or left immature.

CD19$^+$, CD4$^+$, and CD8$^+$ B and T lymphocytes were transfected by using a Genepulser Xcell electroporator (Bio-Rad), as previously described (19), but using DNA instead of RNA. In brief, 2 × 10^6 cells were suspended in 100 μl Opti-MEM (Invitrogen) and electroporated with 15

μg (T cells) or 20 μg (B cells) of DNA in 4-mm electroporation cuvettes. The Genepulser Xcell electroporator (Bio-Rad) was set to square wave, 500 V, 5 ms, and interval 1. After electroporation, cells were cultured 20 h before being harvested for luciferase reporter assays or fluorescence-activated cell sorter (FACS) analyses. Transfection, electroporation, and transduction efficiencies were assessed by using the pGL3/CMV/GFP reporter plasmid.

Transfection of cell lines. XS52, NIH 3T3, or HeLa cells (2×10^5 each) were seeded into 12-well plates (Falcon) and transfected the next day with 2.5 μg DNA, 250 μg/ml DEAE (DEAE cellulose)-dextran (Sigma), and 200 ng/ml chloroquine (Sigma) in a final volume of 200 μl Tris-buffered saline (TBS), using phosphate-buffered saline (PBS)–10% (vol/vol) dimethyl sulfoxide (DMSO; Sigma).

293T cells were transfected by using Lipofectamine LTX with Plus reagent (Invitrogen), according to the manufacturer's protocol, with 0.05 μg pGL3 reporter construct, 0.15 μg each transcription factor construct, and the pcDNA3.1 vector backbone to adjust to 0.5 μg of total DNA. Cells were harvested 48 h after transduction for further analyses.

Recombinant adenoviruses. For a schematic outline of adenoviruses generated in this study, see Fig. 5. Recombinant adenoviruses were first generation, E1 and E3 deleted, replication deficient, and of serotype 5. Virus genomes were obtained by homologous recombination of the corresponding shuttle plasmids containing the different human CD83 promoter-luciferase expression cassettes with pAdEasy-1 in *Escherichia coli* BJ5183, as described previously (18). Adenovirus particles were produced by transfection of PacI-digested pAd plasmids into 293 cells (Quantum) by using Lipofectamine (Invitrogen). The resulting viruses as well as Ad5Luc1 (cytomegalovirus [CMV]-luciferase) and Ad5TL (CMV-luciferase and CMV-green fluorescent protein [GFP]) (18, 20) were amplified in 293 cells (Quantum) and purified by 2 rounds of CsCl equilibrium density gradient ultracentrifugation. Verification of viral genomes and exclusion of wild-type contamination were performed by PCR. The physical particle concentration (viral particles per ml) was determined photometrically (optical density at 260 nm [OD_{260}]), and infectious-particle concentrations were determined by using the 50% tissue culture infective dose ($TCID_{50}$) assay on 293 cells. Ad5Luc1 and Ad5TL were both kindly provided by D. T. Curiel, Birmingham, AL.

Adenoviral transduction of dendritic cells. On day 4, iDCs were transduced with adenoviruses at 500 $TCID_{50}$/cell in a final volume of 250 μl medium, as described previously (18). DCs were stimulated, when indicated, with 0.1 ng/ml LPS (Sigma) for 20 h before being harvested.

Luciferase reporter assay. Luciferase activity was measured by using a luciferase assay system (Promega) according to the manufacturer's instructions but utilizing 50 μl of luciferase assay reagent. Relative light units (RLUs) were obtained with a Wallac Victor instrument (PerkinElmer). RLUs were normalized to the protein concentration, as determined by a Pierce bicinchoninic acid (BCA) protein assay (Thermo Fisher Scientific) according to the manufacturer's protocol.

EMSA. EMSA was performed as described previously (21). In brief, nuclear protein was isolated from iDCs, mDCs matured with LPS for 20 h, and HFF cells by using the nuclear/cytosol fractionation kit (Biovision) according to the manufacturer's protocol. Afterwards, 10 μg of nuclear protein extract was incubated with 4×10^4 cpm of ^{32}P-labeled oligonucleotide coding for the region of interest (three predicted IRF TFBSs and five predicted NF-κB TFBSs). Three micrograms of poly(dI-dC) (Sigma-Aldrich) was included in each reaction mixture as a blocking agent. Wild-type and mutant EMSA probes had identical sequences except for 3 to 5 point mutations (determined by SequenceShaper [Genomatix]). As a cold competitor, a 200× molar excess of unlabeled wild-type or mutant probe was added to the reaction mix. Probes were then loaded onto a nonreducing 6.6% polyacrylamide gel, and the radioactive signal was detected by a fluorescent and radioisotopic image analyzer (FLA-3000 from Raytest) at a 635-nm wavelength. All experiments and stimulations were performed at least in triplicates with cells derived from different healthy donors. Oligonucleotides were purchased from Eurofins MWG Operon, and an-

tibody reagents specific for the following transcription factors were purchased from Santa Cruz Biotechnology (sc) or Abcam (ab): IRF-1 (sc-497x), IRF-2 (sc-498x), IRF-3 (sc-9082x), IRF-4 (sc-6059x), IRF-5 (ab2932), IRF-6 (ab11979), IRF-7 (sc-9083x), IRF-8 (ab28696), p65 (sc-109x), p50 (sc-114x), cRel (sc-70x), RelB (sc-226x), and p52 (sc-298x). As isotype controls, normal rabbit IgG (sc-2027x) and normal goat IgG (sc-2028x) were used.

ChIP. ChIP was performed according to standard procedures (22). In short, cross-linking of iDCs or LPS-matured mDCs (5×10^6 cells each) was performed by incubation for 1 h at room temperature (RT) in 2.5 mM ethylene glycol bis-succinimidylsuccinate (EGS) buffer (Thermo Scientific), followed by further incubation for 30 min in a 10% formaldehyde buffer. Afterwards, cells were washed once with PBS, followed by a freeze-thaw cycle at −80°C and lysis in 300 μl 1% SDS lysis buffer for 10 min on ice. Cell lysates were then sonicated by using a Bioruptor instrument (Diagenode) with 2 times 15 cycles of 30-s on/off intervals on the "high" setting. After centrifugation and passage through a 27-gauge needle, the lysates were transferred into 1.2 ml hypotonic cell lysis buffer containing 0.1% Triton-X. A 50-μl aliquot was removed as the "input" fraction and stored at −20°C until further use. Lysates were then precleared by using 10 μl of washed protein G-coupled magnetic IgG beads (Diagenode). For immunoprecipitation, 2 μg of an antibody specific for IRF-1, IRF-2, p50, p65, cRel, IRF-5, or the rabbit IgG isotype as a control (all antibodies as described above for EMSA) was added to the lysates and incubated for 24 h at 4°C. Afterwards, 25 μl of washed beads was added to the lysates and incubated again for 24 h at 4°C. The next day, beads were washed once consecutively with (i) hypotonic cell lysis buffer, (ii) high-salt buffer containing 500 mM LiCl, (iii) high-salt buffer containing 500 mM LiCl–0.1% SDS, and (iv) Tris-EDTA (TE) buffer, using a magnet to retain beads. The beads were then incubated for 15 min at RT in elution buffer containing 0.1% SDS–0.1 M NaHCO$_3$, heated for 1 min to 65°C, and incubated for 15 min in elution buffer. To reverse cross-linking, 8 μl of a 5 M NaCl solution was added to the input (transferred into 150 μl elution buffer) and the immunoprecipitated fractions, each followed by incubation at 65°C for 24 h. Afterwards, the input and immunoprecipitated fractions were each digested with 100 μg proteinase K (Qiagen), purified by using QIAquick Spin columns (Qiagen) according to the manufacturer's instructions, and finally eluted in 50 μl buffer PB (Qiagen). Precipitated DNA was quantified by qPCR using the Rotor-Gene SYBR green PCR kit (Qiagen), according to the manufacturer's instructions, with 2 μl of the input fraction (prediluted 1:100 in double-distilled water [ddH$_2$O]) and 2 μl of the immunoprecipitated fraction as well as 500 nM each primer (MWG) (primer sequences are indicated in Table S1 in the supplemental material). Data analysis was performed by using Rotor-Gene Q Series software. The cycle threshold (C_T) was determined by the comparative quantification method (23). The percentage of input was determined according to a method described previously by Pfaffl et al. (24) and normalized to the IgG control, which was set to 1. Spacer sequence S1 was used as the control region in ChIP assays to exclude unspecific antibody binding. Regulatory inertness of this region was confirmed by bioinformatic analyses and experimentally by luciferase reporter assays, as shown in Fig. S5 in the supplemental material.

Bioinformatic analysis. All genomic sequences were obtained from the ElDorado database and analyzed by using the Genomatix Suite and programs within (all from Genomatix, Munich, Germany). TFBSs were identified by MatInspector, TFBS frameworks were identified by FastM, and frameworks were searched against sequences in the ElDorado database by using ModelInspector. The mutations of the IRF-binding sites were determined by using SequenceShaper. Phylogenetic analyses were carried out by using RegionMiner and the Common TFBS module of the Genomatix Suite.

Statistical analysis. Prism software was used for statistical analyses (GraphPad). One-way or two-way analysis of variance (ANOVA) with the Bonferroni or Newman-Keuls multiple-comparison *post hoc* test as well as Student's *t* test were used, as indicated, to compare data sets.
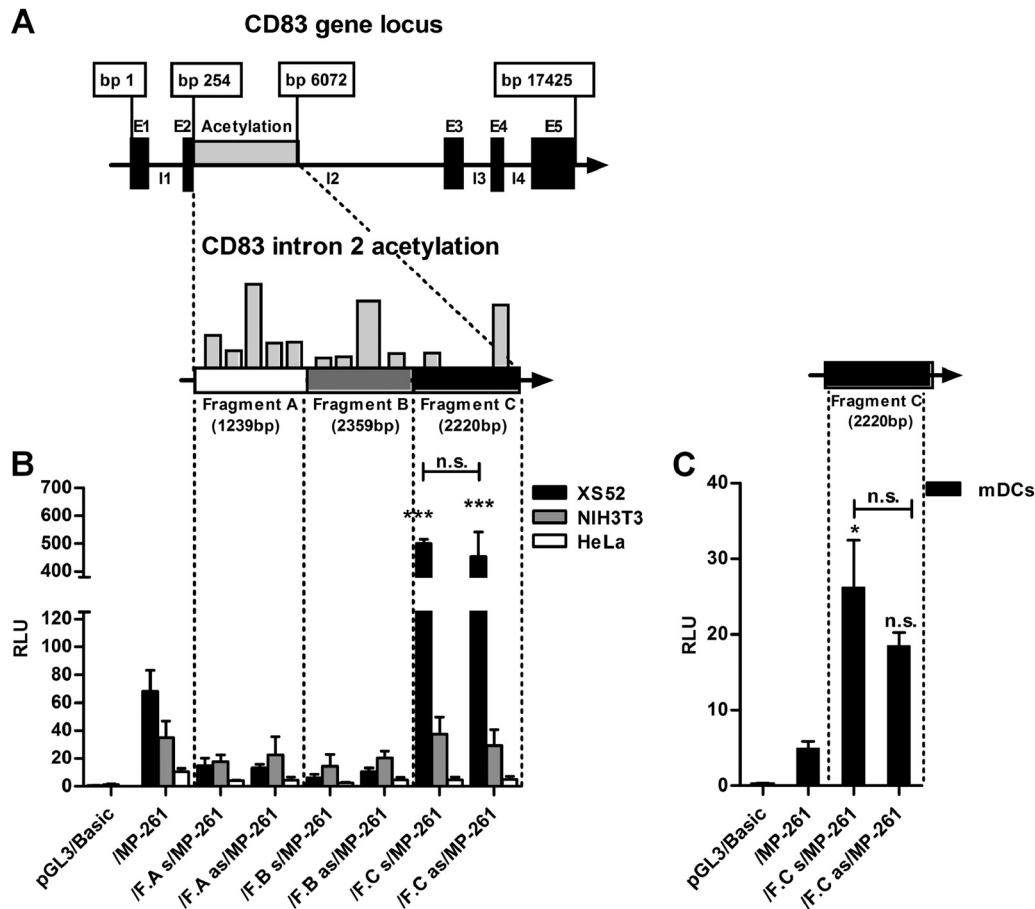
FIG 1 Fragment C of human *CD83* intron 2 enhances MP-261 activity in XS52 cells and mDCs. (A) Schematic depiction of the *CD83* gene locus. The hyperacetylated region of *CD83* intron 2 was subdivided into fragments A (1,239 bp), B (2,359 bp), and C (2,220 bp). (B) Luciferase activity of XS52, NIH 3T3, and HeLa cells transfected with luciferase reporter plasmids, as indicated, containing MP-261 with or without fragment A, B, or C. (C) Luciferase activity of LPS-matured mDCs electroporated with luciferase reporter plasmids containing MP-261 with or without fragment C in the sense or antisense orientation. *, $P < 0.05$; **, $P < 0.01$; ***, $P < 0.001$; n.s. not significant ($P > 0.05$) (determined by one-way ANOVA with Bonferroni [B] or Newman-Keuls [C] multiple-comparison *post hoc* test). Data in panels B and C are means ± standard errors of the means ($n = 3$), with DCs derived from three different donors (C). E, exon; I, intron; F, fragment; s, sense; as, antisense; RLU, relative light units; LPS, lipopolysaccharide; mDCs, mature monocyte-derived dendritic cells.

Approvals and legal requirements for the project. For the generation of PBMCs, monocyte-derived DCs (moDCs), and primary CD19^{+} B and CD4^{+} and CD8^{+} T cells from leukapheresis products of healthy donors, a positive vote from the local ethics committee was obtained (reference number 4261).

RESULTS

The *CD83* gene is hyperacetylated and contains an enhancer in the second intron. Inhibition of acetylation has been described to abrogate CD83 expression during monocyte differentiation into mature DCs (25). We assessed the activation of the human *CD83* gene locus chromatin by a chromatin immunoprecipitation-chip (ChIP-chip) microarray (see Fig. S1 in the supplemental material). This highlighted a relevant hyperacetylated region within the first 6 kb of intron 2 specifically for CD83^{high} mature DCs, which was absent in CD83^{low} immature DCs and CD83[negative] control HFF cells (see Fig. S2 in the supplemental material), after final interpolation of the raw data over 500 bp (see Fig. S1B and C in the supplemental material) using Signal Map software (Roche NimbleGen). Notably, no further acetylated regions could be indentified 150 kb up- and downstream of the human *CD83* gene of

all analyzed cell types (data not shown). To evaluate a potential enhancer element within the 6 kb of the hyperacetylated region, this region was segmented into three smaller fragments, fragment A (FA) (~1.2 kb), fragment B (FB) (~2.3 kb), and fragment C (FC) (~2.2 kb). Single fragments were subsequently cloned into the luciferase reporter vector containing the CD83 core promoter (MP-261), as described previously by S. Berchtold et al. (13) (Fig. 1A; see also Fig. S3 in the supplemental material). Using XS52 murine DC-like cells, significantly enhanced luciferase expression, in comparison to the core promoter alone, was observed for fragment C in the sense and antisense directions (Fig. 1B). However, the luciferase activity was found to be similar to that of MP-261 in NIH 3T3 murine fibroblastic cells and HeLa human cervical carcinoma cells, which both served as controls. Moreover, FA and FB showed no enhancing activity on the minimal promoter MP-261, independent of their orientation and the cell line used. The vector containing MP-261 in combination with FC showed considerably increased luciferase expression in mature primary human monocyte-derived DCs (moDCs) compared to MP-261 alone. For this purpose, moDCs were electroporated with
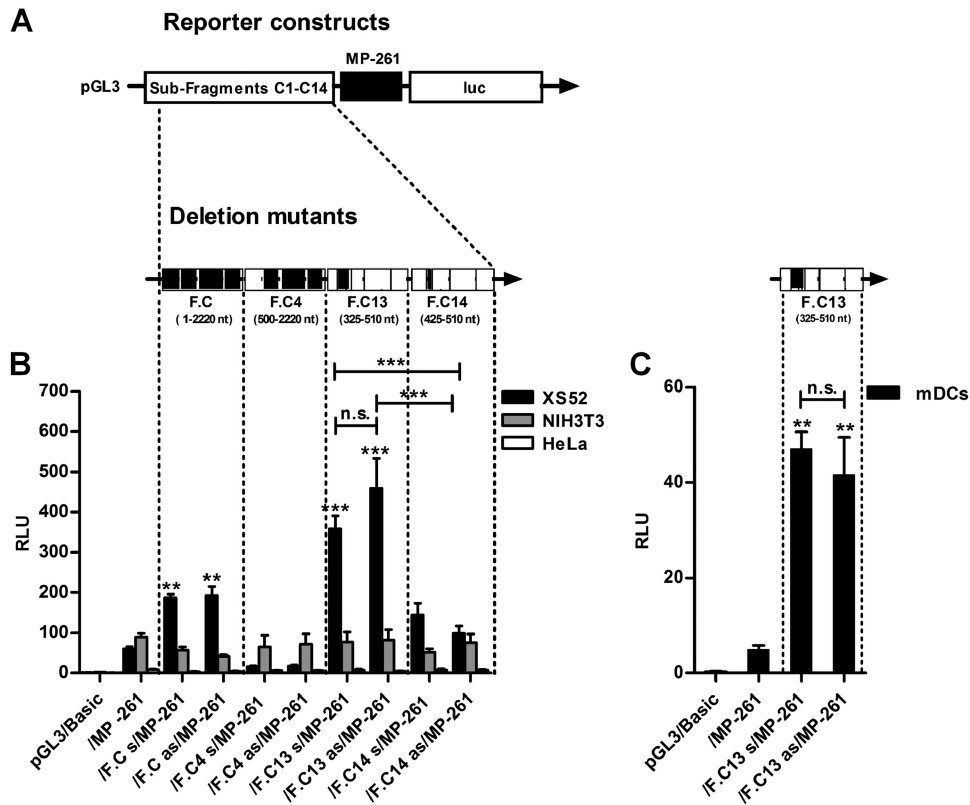
FIG 2 The 185-bp deletion mutant FC13 acts as an enhancer on MP-261 in XS52 cells and mDCs. (A) Deletion mutants FC1 to FC14 of fragment C (see Fig. S3 in the supplemental material) were generated by PCR amplification and cloned in both orientations upstream of MP-261 to asses enhancer function. (B) Luciferase reporter assays of XS52, NIH 3T3, and HeLa cells transfected with luciferase reporter plasmids. Plasmids contained MP-261 with or without fragment C or the deletion mutants FC4, FC13, and FC14 in the upstream position. (C) Luciferase activity of LPS-matured mDCs electroporated with luciferase reporter plasmids containing MP-261 with or without deletion mutant FC13 in the sense or antisense orientation. Statistical significances refer to the activity of the respective MP-261 construct if not indicated otherwise. **, $P < 0.01$; ***, $P < 0.001$; bars without annotation or n.s., not significant ($P > 0.05$) (determined by one-way ANOVA with Bonferroni [B] or Newman-Keuls [C] multiple-comparison *post hoc* test). Data in panels B and C are means ± standard errors of the means ($n = 3$), with DCs derived from three different donors (C). F, fragment; RLU, relative light units; s, sense; as, antisense; LPS, lipopolysaccharide; mDCs, mature monocyte-derived dendritic cells.

the corresponding reporter vectors and matured for 20 h with LPS (mDCs) before luciferase activity was determined by a gene reporter assay (Fig. 1C). These results suggested a cell-type-specific enhancer within FC, which we characterized further by performing serial deletions. FC was truncated in 14 steps to identify a small DNA subfragment that mediates enhancer activity. A summary of all subfragments generated and their activity in XS52, NIH 3T3, and HeLa cells is given in Fig. S4 in the supplemental material. Results from gene reporter analyses of the three most important deletion mutants in comparison to MP-261 alone are shown in Fig. 2A and B. The vector containing FC4, lacking the first 500 bp of FC (nucleotides [nt] 501 to 2220), showed less promoter activity in XS52 cells than MP-261, whereas RLU values remained unaltered in NIH 3T3 and HeLa cells. FC13, comprising a 185-bp subfragment within the first 510 bp (nt 325 to 510) of FC, was demonstrated to induce MP-261 in XS52 cells the strongest in comparison to all other deletion mutants analyzed. Importantly, no enhancement of luciferase activity was observed in control cells after transduction of pGL3/FC13/MP-261. A further decrease in length by 100 bp (FC14 [nt 425 to 510]) resulted in a significant loss of promoter activity in XS52 cells, whereas it was unaltered in NIH 3T3 and HeLa cells. Thus, the enhancer is located within the

185 bp of FC13. Confirmation of FC13 enhancer activity was also performed by electroporation of moDCs, which were afterwards matured for 20 h with LPS (mDCs) before luciferase activity was assessed. Subfragment FC13 (sense and antisense orientations) (Fig. 3C) induced significantly increased luciferase expression together with MP-261 in comparison to MP-261 alone. In summary, we identified a 185-bp enhancer region within the first 6 kb of *CD83* intron 2, which was shown to act in a cell-type-specific manner.

Computational analysis predicts a multifactorial promoter-enhancer region. Next, we addressed the question of how the enhancer could complement the promoter and which transcription factors are involved in this process. A computational analysis of the CD83 promoter region as well as the enhancer predicted three binding sites for NF-κB within MP-261 and two IRF sites within the 185-bp enhancer (Fig. 3). The middle NF-κB site in MP-261 (NF-κB site 4) was functionally confirmed previously by S. Berchtold et al. (13). As NF-κB and IRF are known to cooperate in transcriptional modules (26), we scanned the sequences upstream of the promoter for additional potential binding sites of the two identified candidate TFs, i.e., NF-κB and IRF. A third IRF-binding site was predicted about 250 bp upstream of MP-261,
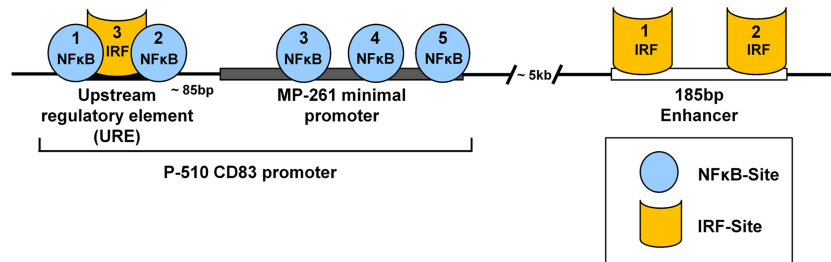
FIG 3 Model of the CD83 promoter-enhancer region, including bioinformatically predicted transcription factor-binding sites. All genomic sequences were obtained from the ElDorado database and analyzed by using the Genomatix Suite. Transcription factor-binding sites (TFBSs) were identified by MatInspector. Shown is a depiction of the three defined regions with the putative transcription factor-binding sites regulating CD83 transcription: the URE (NF-κB sites 1 and 2 and IRF site 3), MP-261 (NF-κB sites 3, 4, and 5), and the enhancer (IRF sites 1 and 2). The combination of the URE and MP-261 in the genomic configuration was termed P-510.

which, together with two further (weak) NF-κB-binding sites, could represent an upstream regulatory element (URE). In summary, the computational analyses of the *CD83* gene suggested a 510-bp CD83 promoter (P-510) consisting of the URE and MP-261, which is supposed to cooperate with the 185-bp enhancer.

CD83 expression is regulated in a cell-type- and maturation-specific manner. We generated reporter vectors containing either P-510 alone or in combination with the 185-bp enhancer (P-510/E_s or P-510/E_as) in order to verify our hypothetical promoter-enhancer model. A spacer sequence of approximately 500 bp (S1) was inserted between MP-261 or P-510 and the enhancer (see Fig. S5A in the supplemental material), to allow looping of the enhancer onto the promoter. The spacer did not influence the promoter activity on its own (see Fig. S5B to D in the supplemental material). Subsequently, we compared the activities of the tripartite P-510/S1 and the two-part MP-261/S1 vectors by luciferase reporter assays. The results confirmed the specific enhancer activity of the 185-bp fragment. Although the tripartite reporter vectors exhibited a slightly enhanced activity in DC-like XS52 cells in comparison to the two-part constructs (see Fig. S5B in the supplemental material), this was not significant ($P > 0.05$). This effect might be due to multiple *trans* complementations possible in transient-expression assays, substituting for intramolecular folding in *cis*; e.g., one promoter interacted with two enhancers. To avoid this confounding effect, we generated adenoviral vectors corresponding to the above-described reporter vectors (Fig. 4A). This provided a native chromatin-like structure ensuring *cis* arrangement of the promoter-enhancer region. Next, immature moDCs were transduced with the recombinant adenoviruses, either matured with LPS or not. Twenty hours afterwards, cells were harvested for luciferase reporter assays. No differences in immature or mature DCs were found between Ad/S1/MP-261 and (i) Ad/S1/P-510 lacking the 185-bp enhancer as well as (ii) Ad/Enh/S1/MP-261 containing the enhancer in either the sense or antisense direction (Fig. 4A). However, a significant increase in promoter activity was observed regarding the tripartite vector Ad/Enh/S1/P-510 containing the enhancer (in either the sense or antisense direction), the URE, and the minimal promoter in comparison to the two-part vectors lacking the URE. Moreover, these tripartite vectors also showed a significant difference in luciferase induction between immature and mature DCs, indicating a cell-type- and maturation-specific activity of this promoter-enhancer construct. In contrast, luciferase expression was completely abrogated in the absence of the promoter (Ad/Enh/S1). To address the cell-type-

specific activity of the CD83 promoter complex region, we transduced lymphocytic Raji, Jurkat, and JCAM cells (see Fig. S6B to D in the supplemental material), which upregulate CD83 surface expression after stimulation (data not shown), with the adenoviral vectors mentioned above. Although the overall promoter activity was higher in all three cell lines after stimulation, no differences in luciferase expression could be observed between the vectors containing and those lacking the enhancer, neither for unstimulated nor for stimulated cells.

To confirm this finding in primary lymphocytes, we isolated primary CD19$^+$ B cells as well as CD4$^+$ and CD8$^+$ T cells and stimulated them with either pokeweed mitogen (B cells) or PHA-P plus IL-2 (T cells). Subsequently, cells were analyzed for CD83 expression (data not shown) and electroporated with the corresponding tripartite and control reporter vectors used in the experiments described above. The vector containing only P-510 showed the highest activity in all three cell types (Fig. 5B to D). In contrast, the tripartite region additionally comprising the enhancer (in either the sense or antisense direction) induced luciferase expression in B and T cells to a lesser extent than P-510 alone. Again, no luciferase expression was measured in the absence of the promoter (Enh/S1). Hence, these data demonstrate the cell type and maturation specificity of this newly identified extended promoter-enhancer transcription region.

NF-κB TFs p50, p65, and cRel and IRF-1, IRF-2, and IRF-5 bind to the CD83 promoter complex. We next investigated the binding of the TFs of the NF-κB and IRF family to the computationally predicted TFBSs (Fig. 3) by EMSA and ChIP analysis. First, nuclear extracts from iDCs, mDCs, and HFF cells were generated to be used in mobility shift assays in the absence of NF-κB- and IRF-specific antibodies (see Fig. S7 in the supplemental material). The results here demonstrate that all proposed NF-κB (see Fig. S7A) and IRF (see Fig. S7B) TFBSs were bound by a nuclear protein in mDCs. The same was observed for iDCs, except for the weak NF-κB site 2, which was not bound by a nuclear protein. However, HFF control cells showed binding of nuclear factors only to NF-κB sites 1 and 3 and no further binding to the remaining NF-κB and IRF sites. To identify the exact subunit of the corresponding NF-κB and IRF TF family members, antibody-mediated supershifts against NF-κB subunits p50, p65, cRel, RelB, and p52 (Fig. 5A, lanes 3 to 7; see also Fig. S8A to C in the supplemental material) as well as IRF family members IRF-1 to IRF-8 (Fig. 5B, lanes 3 to 10; see also Fig. S8D to G in the supplemental material) were performed with nuclear extracts from iDCs and
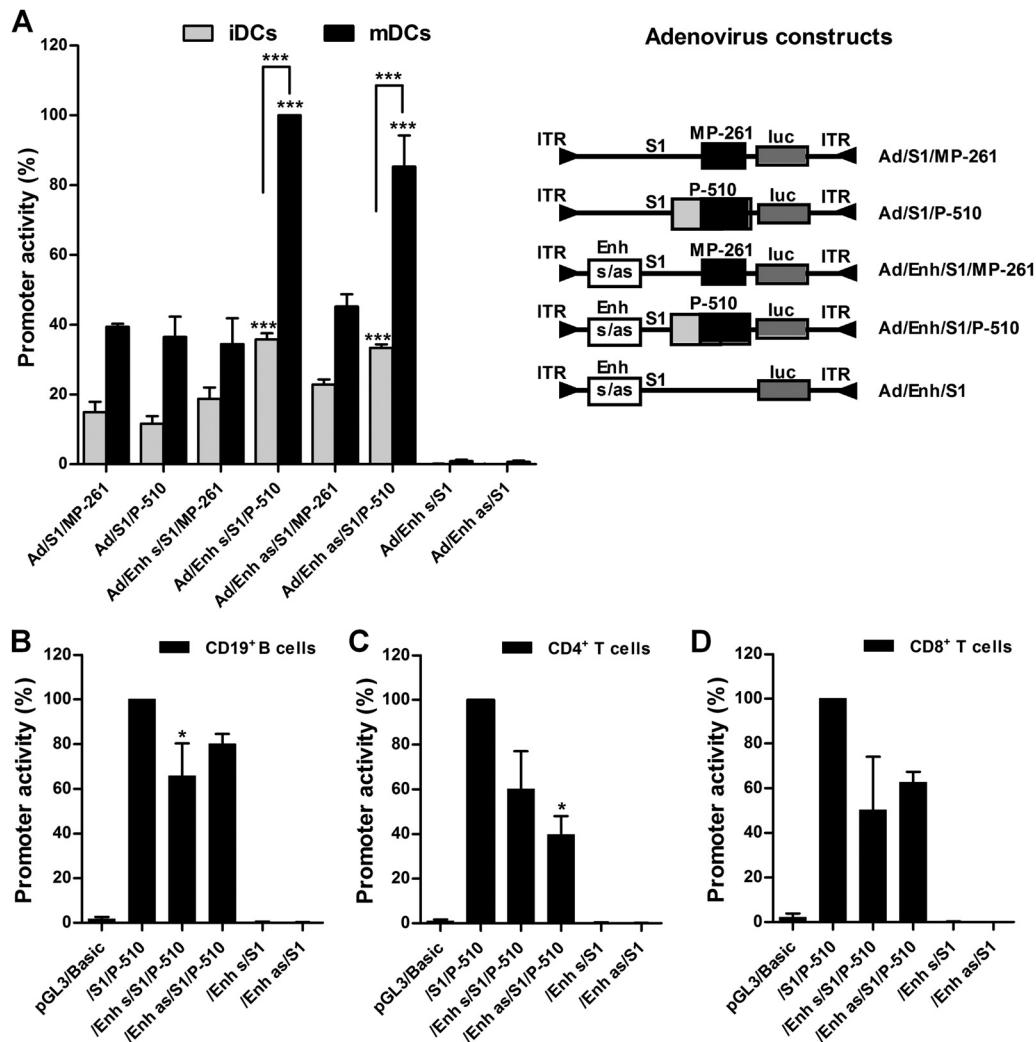
FIG 4 The ternary complex of the URE, MP-261, and the enhancer acts in a cell-type- and stadium-specific manner. (A) Luciferase activity of iDCs and mDCs. Immature DCs were transduced with adenoviral vectors at 500 TCID$_{50}$/cell, as indicated, and subsequently matured with LPS for 20 h. (B to D) Luciferase activity of human primary CD19^{+} B cells (B) and CD4^{+} (C) and CD8^{+} (D) T cells. CD19^{+} B cells were cultivated for 5 days and CD4^{+} and CD8^{+} T cells were cultured for 2 days in the presence of PHA-P and IL-2. Cells were subsequently electroporated with luciferase reporter constructs, as indicated (see Fig. S4A in the supplemental material). The strongest promoter activity was achieved with Ad/Enh_s/S1/P-510 (A) or pGL3/S1/P-510 (B to D) and was therefore set to 100%. Statistical significances refer to the activity of the respective MP-261 (A) or P-510 (B to D) construct if not indicated otherwise. *, $P < 0.05$; ***, $P < 0.001$; bars without annotation are not significant ($P > 0.05$) (determined by one-way and two-way ANOVA with Bonferroni multiple-comparison *post hoc* test). Data are means ± standard errors of the means ($n = 3$), with cells derived from different donors. ITR, inverted terminal repeat; luc, luciferase; Enh, enhancer; S1, spacer sequence; F, fragment; s, sense; as, antisense; RLU, relative light units; LPS, lipopolysaccharide; iDCs, immature monocyte-derived dendritic cells; mDCs, mature monocyte-derived dendritic cells; TCID, tissue culture infective dose.

mDCs. For the URE, we demonstrated a binding of an as-yet-unspecified factor in iDCs and mDCs to NF-κB site 1 as well as NF-κB site 2 only in mDCs. NF-κB site 2 binding was observed only in mDCs, whereas IRF-5 attached to IRF site 3 in iDCs and mDCs. NF-κB sites 3, 4, and 5 (all within MP-261), however, were bound by p50 in both iDCs and mDCs. Moreover, we found cRel as a binding partner in NF-κB site 4 and in mDCs, while for iDCs, the signal was very weak and not significant (Fig. 5A; see also Fig. S9A in the supplemental material). Regarding the enhancer, IRF site 1 was bound mainly by IRF-2 in iDCs, whereas supershifts in mDCs indicated a stronger signal for IRF-1 together with a decreased binding intensity for IRF-2 (see also additional donors in Fig. S8D and E in the supplemental material). Finally, IRF site 2

(within the enhancer) was found to bind an as-yet-unknown TF in iDCs as well as in mDCs. These results were confirmed by further EMSAs with DCs derived from different donors, as outlined in Fig. S8 in the supplemental material, and by a corresponding evaluation of all EMSA experiments performed by using AIDA Image Analyzer software (see Fig. S9 in the supplemental material). To demonstrate the presence of the TFs p50, p65, cRel, IRF-1, IRF-2, and IRF-5 also at the endogenous site *in vivo*, ChIP analyses against the indicated TFs were performed (Fig. 6). Thereby, the control spacer S1 region (Fig. 6B) described above showed no binding of any of the TFs in iDCs and mDCs. In the URE (Fig. 6C), however, p50, p65, and cRel were found to bind in iDCs and also, to a much greater extent, in mDCs. Furthermore, IRF-1 and IRF-5
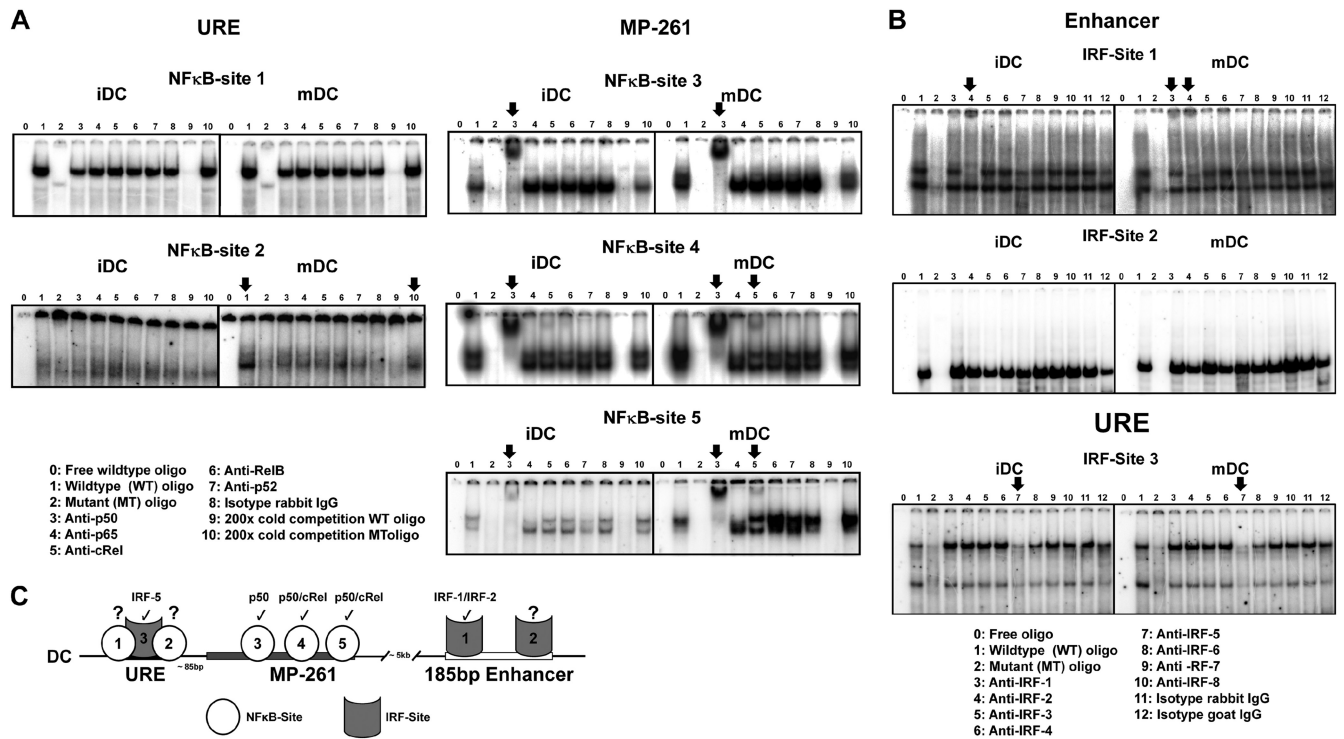
FIG 5 NF-κB and IRF TFs bind to the bioinformatically predicted TFBSs. (A) EMSA performed with nuclear extracts derived from iDCs or 20-h-LPS-matured mDCs and incubated with ^{32}P-end-labeled double-stranded wild-type (lanes 0, 1, and 3 to 10) or mutant (lane 2) oligonucleotides coding for predicted NF-κB sites 1 to 5. Lanes 3 to 7 show band shift reaction mixtures that were incubated additionally with antibodies against the NF-κB family member p50, p65, cRel, RelB, or p52. The rabbit IgG isotype (lane 8) and a 200× molar excess of wild-type (lane 9) and mutant (lane 10) cold-competition oligonucleotides have also been included as controls. (B) EMSA performed as described above for panel A. Wild-type (lanes 0, 1, and 3 to 10) or mutant (lane 2) oligonucleotides code for predicted IRF sites 1, 2, and 3. Lanes 3 to 10 show band shift reaction mixtures that were incubated additionally with antibodies against the members of the IRF family (IRF-1 to IRF-8). Rabbit or goat IgG isotypes (lanes 11 and 12, respectively) are also included. For cold-competition controls, see Fig. S8 in the supplemental material. One representative experiment out of at least three independently performed experiments representing different donors is shown. An arrow indicates a binding reaction (supershift and/or decrease in band shift intensity). (C) Overview of predicted TFBSs and summary of EMSA results from iDCs and mDCs. ✔, verified binding site; ?, binding by a not-yet-identified factor.

were present only in mDCs, while IRF-2 was detectable only in iDCs. MP-261 (Fig. 6D) was shown to bind not only p50 in iDCs but also cRel especially in mDCs. Additionally, p65 was found to bind to MP-261 in mDCs. Enhancer binding of IRF-5 in both iDCs and mDCs as well as of IRF-2 only in iDCs was detected. Taken together, these results underline the importance of p50, p65, cRel, IRF-1, IRF-2, and IRF-5 for the regulation of CD83 promoter activation determined by both EMSA and ChIP analysis.

Next, we analyzed the expression pattern of the TFs IRF-1, IRF-2, IRF-5, p50, p65, and cRel by three independent experiments with nuclear extracts of iDCs, mDCs, and HFF cells using Western blotting, followed by AIDA evaluation (see Fig. S10 in the supplemental material). Here we found weak expression of NF-κB TFs p50, p65, and cRel in HFF cells and iDCs, which greatly increased in mDCs. Moreover, IRF-1 was detected only in mDCs, whereas IRF-2 was found in all three cell types although to a much lesser extent in HFF cells. IRF-5 was demonstrated to be expressed only in nuclei of iDCs and mDCs. In summary, results of EMSA, ChIP, and AIDA quantifications confirmed the computationally predicted TFBSs in the CD83 promoter sequence as well as their actual binding by NF-κB and IRF factors, supported by Western blot analyses of TF expression in DCs and HFF cells.

The NF-κB and IRF TFBSs are essential for transcriptional activation. Based on the results described above, we analyzed the

TF-binding properties of the predicted NF-κB sites within the URE and MP-261 of the three identified regulatory regions of CD83. CD83-negative 293T cells were cotransfected with reporter constructs containing either the URE (Fig. 7, left; see also Fig. S11 in the supplemental material) or MP-261 (Fig. 7, right), both lacking the enhancer, together with vectors coding for NF-κB TFs involved in the canonical pathway, p50, p65 (RelA), cRel, as well as IRF-5. While p50 alone did not induce the URE, p65 or IRF-5 alone as well as p50/p65 or p50/IRF-5 slightly enhanced the transcriptional activity. In contrast, the combinations of p65/IRF-5 as well as p50/p65/IRF-5 significantly increased URE activity in comparison to the URE alone. Interestingly, mutation of the respective IRF site in the URE clearly abrogated this effect (see Fig. S11 in the supplemental material). MP-261, however, was not significantly induced by p50, cRel, p50/cRel, IRF-5, and p50/IRF-5 in comparison to MP-261 alone (Fig. 7, right). Conversely, cotransfection with cRel/IRF-5 resulted in a significant increase of luciferase activity, which could not be increased further by the addition of p50. Interestingly, the strongest induction of MP-261 was achieved by the cotransfection of p65, which decreased in the presence of p50 and further increased in the presence of IRF-5. Taken together, these data identified the TFs p65, cRel, and IRF-5 to be highly involved in the regulation of human CD83 promoter activity. p65 and IRF-5 clearly showed a more-than-additive synergistic effect.
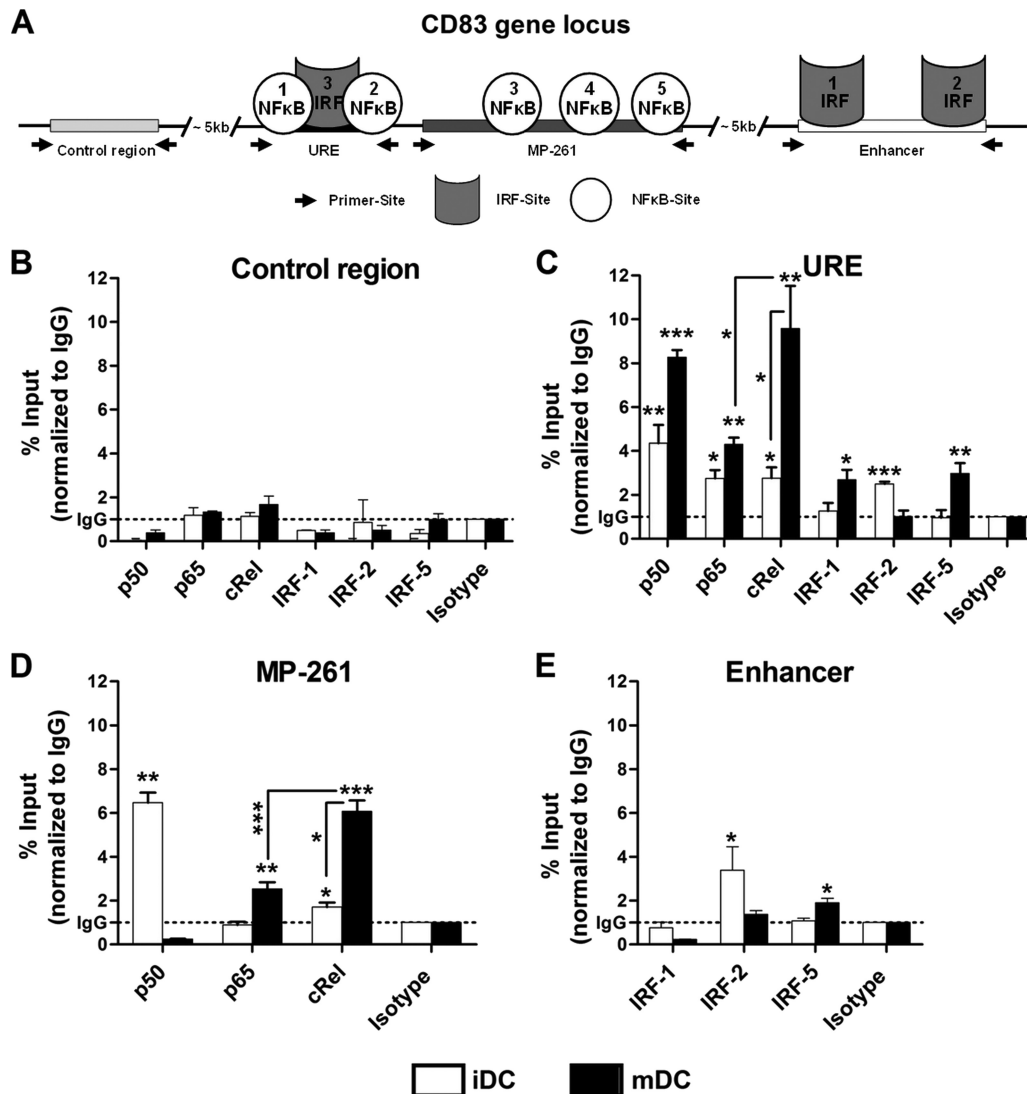
FIG 6 Chromatin immunoprecipitation (ChIP) confirms binding of NF-κB and IRF TFs to the CD83 gene locus. (A) Schematic depiction of the CD83 gene locus comprising the URE, MP-261, and the enhancer. The control region for ChIP is located approximately 5 kb upstream of the CD83 gene locus. (B to D) ChIP performed with lysates of 5×10^6 iDCs or LPS-matured mDCs cross-linked with EGS, lysed, sonicated, and subsequently immunoprecipitated with antibodies, as indicated. Analyses of specific antibody-dependent enrichment in comparison to not-precipitated "input" DNA were performed via SYBR green-qPCR using primers for the control region (B), the URE (C), MP-261 (D), and the enhancer (E). Bars indicate percent enrichment compared to the input DNA and were normalized to the isotype control (IgG). Statistical significances refer to percent enrichment of the respective isotype control if not indicated otherwise. *, $P < 0.05$; **, $P < 0.01$; ***, $P < 0.001$; bars without annotation are not significant ($P > 0.05$) (determined by one-way ANOVA with Bonferroni multiple-comparison *post hoc* test [B to E] and Student *t* test for the comparison of two values [C to E]). Data shown are means ± standard errors of the means ($n = 3$), with DCs derived from different donors. LPS, lipopolysaccharide; iDC, immature monocyte-derived dendritic cells; mDC, mature monocyte-derived dendritic cells; URE, upstream regulatory element; MP-261, minimal promoter 261; IRF, interferon regulatory factor.

Next, discrete point mutations were introduced into reporter vectors containing P-510 and the 185-bp enhancer in order to further assess the involvement of the three IRF-binding sites within the URE and the enhancer of the CD83 promoter complex. IRF-binding site 1, 2, or 3 was destroyed by mutation separately or in combination. Either both sites within the enhancer or all three sites within the promoter-enhancer region were mutated (Fig. 8; see also Fig. S12A in the supplemental material). Subsequent luciferase reporter assays revealed a clear loss of promoter activity in comparison to the corresponding nonmutated constructs in XS52 cells (see Fig. S12B in the supplemental material) as well as in human mature DCs (Fig. 8). In the absence of the enhancer, the

mutation of IRF site 3 within the URE showed no changes in transcriptional activation. However, a significant loss was observed for constructs containing the enhancer. Destruction of one of the two IRF sites within the enhancer led to a strongly reduced promoter activity, which was further decreased by mutating both IRF sites simultaneously. As expected, the complete destruction of all three IRF sites within the URE and the enhancer led to a similar result as the double mutation within the enhancer. To further clarify the relevance of IRF site 3 within the URE, constructs containing the URE were compared with either vectors bearing a mutation (URE/IRF site 3 mutation) or the promoterless pGL3/Basic vector (see Fig. S12C in the supplemental material). Notably, the presence of the URE alone
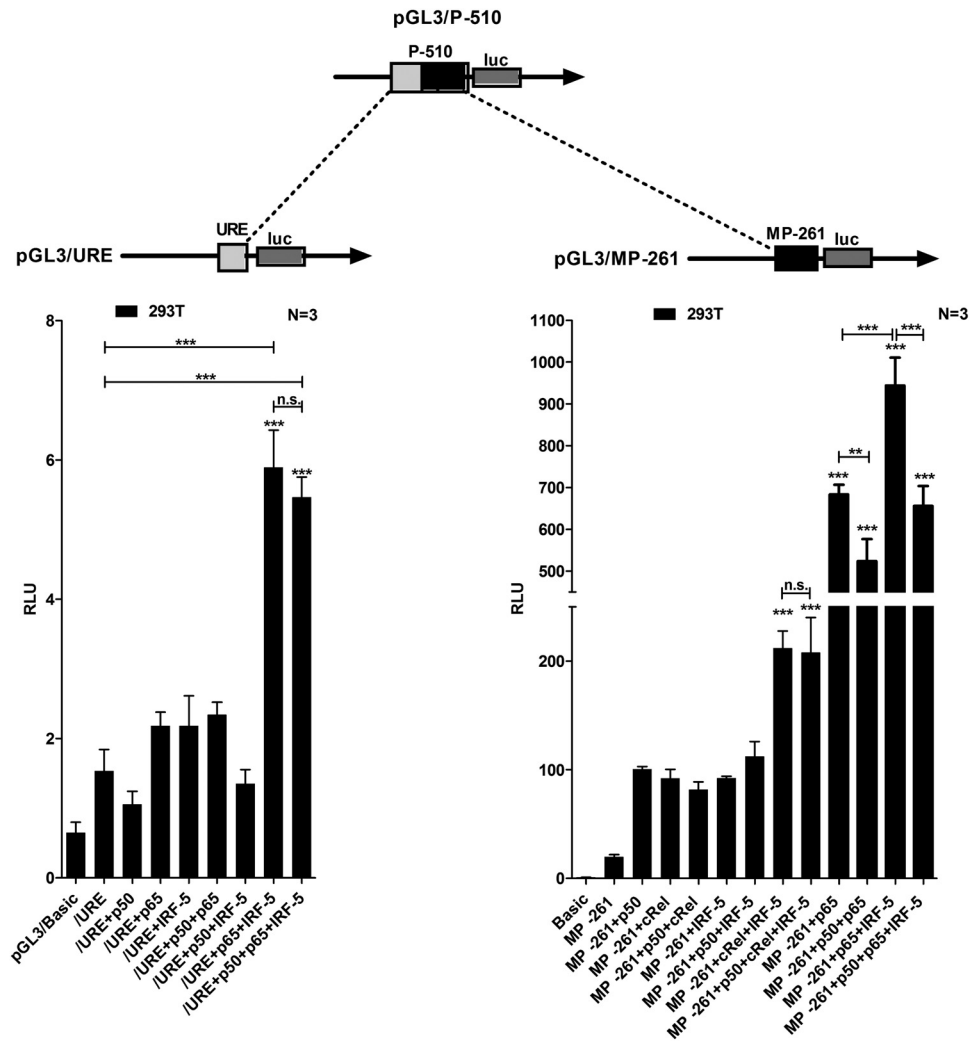
FIG 7 Transcription factors of the NF-κB and IRF family induce the URE and MP-261 in 293T cells. Shown are luciferase activities of 293T cells. Cells were cotransfected with luciferase reporter plasmids containing either the URE (left) or MP-261 (right) and expression plasmids coding for NF-κB and IRF subunits p50, p65, cRel, and IRF-5 or a combination thereof. Cells were lysed after 48 h for luciferase reporter assays. Statistical significances refer to the activity of the respective URE or MP-261 construct if not indicated otherwise. *, $P < 0.05$; **, $P < 0.01$; ***, $P < 0.001$; n.s., not significant ($P > 0.05$) (determined by one-way ANOVA with Bonferroni multiple-comparison *post hoc* test). Data shown are means ± standard errors of the means ($n = 3$). RLU, relative light units; luc, luciferase.

led to significantly enhanced promoter activity, which dropped down to background values after disruption of IRF site 3, indicating its importance for the tripartite structure.

DISCUSSION

A 261-bp fragment upstream of the ATG translational start site containing a NF-κB-binding site was previously shown to regulate CD83 expression in different cell types. However, this minimal promoter was neither cell type nor activation/maturation specific (13). We report here for the first time a human cell-type- and maturation-specific promoter complex regulating CD83 expression in mature DCs. Using ChIP-on-chip analyses and bioinformatic approaches, we identified a transcriptional module consisting of a proximal promoter of 164 bp, located 85 bp upstream of the minimal promoter (261 bp), and a downstream enhancer (185 bp) within intron 2 of the *CD83* gene working synergistically in *trans*. By conducting *in vitro* promoter reporter gene analyses in

human DCs, CD19+ B cells, and CD4+ and CD8+ T cells as well as in different cell lines, we found this module to drive highly specific gene expression only in mature DCs. Previously, the human fascin promoter was reported to be active in mature human DCs (27). However, fascin is expressed not only by mature DCs but also by neuronal and glial cells (28) and capillary endothelial cells (29) and is strongly upregulated in most forms of human carcinoma (30). In this respect, it has been shown that a 3.1-kb 5′-flanking region of human *fascin-1* induces reporter genes not only in mature human DCs but also in other nontransformed fascin-positive cells (31). Thus, the human CD83 regulatory unit described here is the first specific one for mature DCs only, which therefore opens new therapeutic strategies for the *in vivo* targeting of mature DCs, e.g., in cancer patients.

Using bioinformatic approaches, five NF-κB and three IRF TFBSs have been found to be involved in these three regions regulating the transcription of the *CD83* gene. Indeed, Toll-like re-
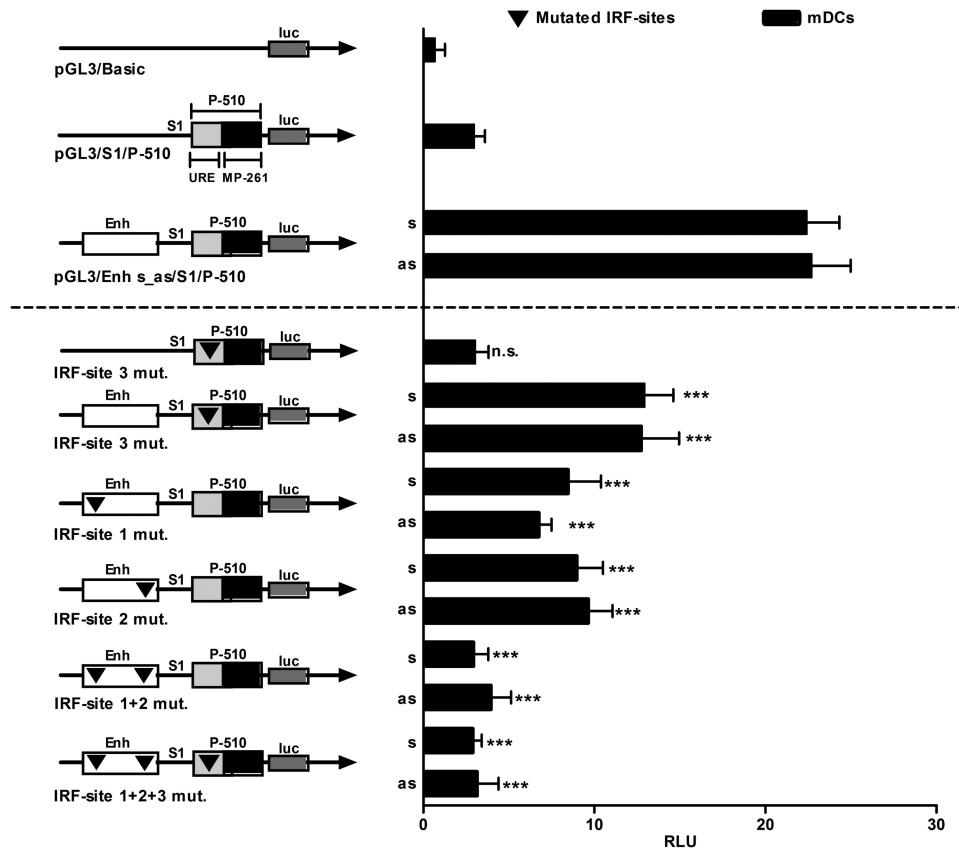
FIG 8 Mutation of any of the three interferon regulatory factor (IRF)-binding sites in the ternary complex significantly reduces luciferase expression in mDCs. Shown are luciferase activities of 20-h-LPS-matured mDCs electroporated with luciferase reporter plasmids containing P-510 with or without the 185-bp enhancer containing either wild-type or mutated IRF sites. Predicted IRF sites in P-510 and the 185-bp enhancer were mutated in different combinations by using site-directed PCR mutagenesis and statistically compared to the corresponding not-mutated constructs. ∗∗, $P < 0.01$; ∗∗∗, $P < 0.001$; n.s., not significant ($P > 0.05$) (determined by one-way ANOVA with Bonferroni multiple-comparison *post hoc* test). Data shown are means ± standard errors of the means ($n = 3$), with cells derived from three different donors. Mutations are indicated by a black triangle. Enh, enhancer; luc, luciferase; S1, spacer sequence; s, sense; as, antisense; RLU, relative light units; mDCs, mature monocyte-derived dendritic cells; IRF, interferon regulatory factor.

ceptor 4 (TLR-4) triggering by LPS induces the MyD88-dependent and Trif-dependent pathways, resulting in the activation of canonical NF-κB and IRF TFs (32). In this context, we showed by EMSA and ChIP analyses that IRF-5 binds to the URE, p50 and cRel bind to MP-261, and IRF-2 binds to the enhancer. Notably, binding of cRel, IRF-2, and IRF-5 was maturation dependent. Differences between results obtained especially for iDCs and mDCs by EMSA and ChIP analyses might be explained by the disparity of these two methods. In EMSA, TFBSs are analyzed out of context, meaning that the binding site is not in an endogenous "*in vivo*" environment, thereby potentially preventing cooperative binding of different TFs, independent of the maturation status of the DC. Cross-linking of endogenous chromatin complexes during ChIP, however, might lead to the coprecipitation of transactivating TFs that are in close proximity at that time point. Moreover, cotransfection experiments in 293T cells identified that the combination of p65 or cRel with IRF-5 resulted in the strongest induction of the URE and MP-261, which is clearly in line with results shown by ChIP. Furthermore, this is in accordance with data reported previously by the group of Irina Udalova, which indicated that p65 induces basal transient transcriptional activity of the TNF-α promoter in DCs (33). Regarding their model, IRF-5 is first recruited to an upstream interferon regulatory element

(ISRE) flanked by a NF-κB site upon LPS stimulation, which then interacts at another downstream NF-κB site directly with p65, resulting in an upregulated and prolonged induction of TNF-α expression. Additionally, IRF-5 was recruited to a NF-κB site via direct interaction with p65. Moreover, the NF-κB dependency for CD83 expression has also been described by other groups (13, 34). IRF-5, however, is expressed constitutively in DCs but has been described to be expressed as multiple splice variants with distinct cell-type-specific expression and cellular localization, differential regulation/activation, and dissimilar functions (35–37). Although the functions of IRF-5 are not yet fully elucidated, it has been shown by the group of Irina Udalova to coinduce (i) gene expression in immune cells as an upstream promoter-binding factor (33) and (ii) CD83 expression in DCs after adenovirus-mediated overexpression (38), thereby indicating that IRF-5 is a factor for the fine regulation of human CD83 expression. Whereas a strong binding of an as-yet-unknown TF was observed for IRF site 2, IRF-1 and -2 were specified by EMSA to bind to IRF site 1 within the enhancer. Interestingly, ChIP analysis confirmed only the binding of IRF-2 to the enhancer in iDCs but additionally showed binding of IRF-2 and IRF-1 to the URE in iDCs and mDCs, respectively. Thereby, IRF-1 and -2 not only are considered to be essential mediators of DC development and function (39–41) but

also are able to bind to the same TFBSs (42, 43). Hence, they regulate gene expression in an antagonistic manner by competing for the same TFBS, with IRF-1 as a transcriptional activator and IRF-2 as a repressor (44). Moreover, it has been reported that both IRF-1 and IRF-2 interfere with histone acetylation (45): the repressive function of IRF-2 is partially attributed to its ability to inhibit acetylation of core histone chromatin, which leads to a closed conformation (46). IRF-1, on the other hand, is able to recruit histone acetyltransferases that in turn acetylate core histones, leading to an open conformation of the chromatin, which allows the binding of transcription factors as well as DNA looping to establish, e.g., enhancer-promoter interactions (47).

To further verify the importance of the three IRF TFBSs, the respective binding sites in the URE and the enhancer were altered by individual or multiple point mutations. The SequenceShaper tool (48) (Genomatix, Munich, Germany) was used to design the point mutations ensuring the elimination of the TFBSs, thereby preventing the generation of new TFBSs as a result of the mutation. Elimination of any of the IRF TFBSs led to a significant loss of reporter activity, additionally highlighting their importance for the transcriptional regulation of the *CD83* gene. This is in accordance with previous reports showing that IRF TFs are involved in the activation of genes encoding proinflammatory cytokines like IL-6, IL-12, and TNF-α (33, 49) as well as of costimulatory molecules like CD40 and CD86 (38).

While there is now solid experimental evidence for the functional involvement of all three regions (enhancer, URE, and MP-261), there is no proof for any mechanism of how these three regions can cooperate. Closer examination of the internal distances of the crucial NF-κB and IRF TFBSs as well as evidence from the literature about known transcriptional modules involving NF-κB and IRF TFBSs lead us to propose a (at this point) hypothetical model: the internal distances of the predicted (and verified) TFBSs within the three regions suggested a possible *trans*-complementation model in which the enhancer interacts with MP-261 by forming an intrachromosomal loop, a well-known process involved in transcription (50, 51), whereas the URE is brought into close alignment with MP-261 (Fig. 9). At present, however, we have no experimental data proving or disproving this hypothesis. The distance of 203 bp would allow nucleosome binding, but short-range loop formations by TFs have been experimentally observed, with loop sizes as small as 116 bp *in vitro* as well (52). Hence, this model is fully compatible with all theoretical and experimental facts and is further supported by known NF-κB and IRF interactions.

NF-κB and IRF are known to act synergistically in a variety of transcriptional modules (see reference 53 and references therein) (MatBase; Genomatix, Munich, Germany), such as NF-κB–IRF in the promoter of the human HLA B gene (54) or the IRF–NF-κB module in the murine IP-10 promoter (55). However, such modules usually contain both types of TFBSs in *cis*, ensuring the proper arrangement of the binding proteins. In the case of the human CD83 promoter, we found a physical separation of the NF-κB and IRF TFBSs into three distinct regions, the enhancer, the URE, and the minimal promoter (MP-261). It is remarkable that the relative location of the NF-κB and IRF sites within the URE was inversed with respect to the promoter organization, ensuring an almost perfect juxtapositioning of the respective sites upon direct backfolding of the upstream regulatory element onto the minimal promoter. The enhancer contributing two IRF TFBSs was supposed
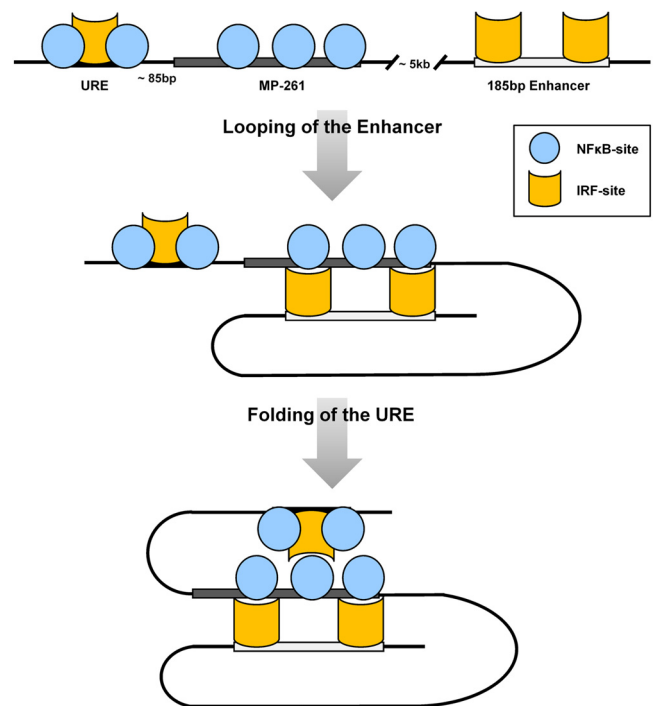

FIG 9 Hypothetical folding model of the interaction of the CD83 upstream regulatory element (URE), the CD83 minimal promoter (MP-261), and the 185-bp enhancer. All genomic sequences were obtained from the ElDorado database and analyzed by using the Genomatix Suite. Transcription factor-binding sites (TFBSs) were identified by MatInspector, and TFBS frameworks were identified by FastM. Shown is the proposed formation of the CD83 regulatory unit consisting of the URE (NF-κB sites 1 and 2 and IRF site 3), MP-261 (NF-κB sites 3, 4, and 5), and the enhancer (IRF sites 1 and 2). NF-κB subunits at MP-261 interact with IRF factors at the 185-bp enhancer via looping of the DNA. The IRF–NF-κB complex at the URE then interacts with the NF-κB units at MP-261 by folding back, leading to a transcriptional module formed in *trans*. The proposed hypothetical model is in line with experimental evidence obtained for mDCs in this study. IRF, interferon regulatory factor.

to work in both directions due not only to the potential looping of the sequences but also to the internal symmetry. The setup of IRF and NF-κB sites was apparently unique in the human genome, as no other such constellation could be found in a database search with a computational model of the construct (ModelInspector) (48). However, similar setups with enhancer (IRF) and promoter (NF-κB) sites lacking the URE part could be located in a few other cases. Interestingly, the enhancer-promoter setup was phylogenetically conserved in several mammalian species (human, macaque, chimpanzee, mouse, rat, and pig) (data not shown), but no other species had a similar URE setup. Thus, it appeared that the CD83 maturation-specific URE–MP-261 enhancer region is quite unique and is most likely the cleanest system for stage-specific expression, at least in mature or maturing DCs. Moreover, the discovery of this unique regulatory unit of three regions offers new means for proactive promoter database searches to specify novel genes with similar promoter organizations in general, once candidate binding sites have been identified. Such an approach has been successfully applied to identify functionally related genes via promoter analysis in podocyte tight junction complexes (17).

In summary, we identified a DC- and maturation-specific CD83 promoter comprising a regulatory unit of three regions, a URE, a minimal promoter (MP-261), and a downstream en-

hancer containing IRF and NF-κB TFBSs working most likely synergistically in *trans*. Although the involvement of species- and cell-type-specific factors in *CD83* gene expression still have to be elucidated in future studies, we report IRF-1, IRF-2, IRF-5, p50, p65, and cRel to be directly involved in transcriptional activation. Finally, an understanding of promoter formation and gene regulation of maturing DCs will help to identify novel mechanisms linked in a regulatory network of DC activation and their function and allow for transcriptional targeting of DCs.

ACKNOWLEDGMENTS

REFERENCES

1. **Bancherau J, Steinman RM.** 1998. Dendritic cells and the control of immunity. Nature **392**:245–252.

2. **Zhou LJ, Tedder TF.** 1996. CD14+ blood monocytes can differentiate into functionally mature CD83+ dendritic cells. Proc. Natl. Acad. Sci. U. S. A. **93**:2588–2592.

3. **Prechtel AT, Steinkasserer A.** 2007. CD83: an update on functions and prospects of the maturation marker of dendritic cells. Arch. Dermatol. Res. **299**:59–69.

4. **Kruse M, Rosorius O, Kratzer F, Bevec D, Kuhnt C, Steinkasserer A, Schuler G, Hauber J.** 2000. Inhibition of CD83 cell surface expression during dendritic cell maturation by interference with nuclear export of CD83 mRNA. J. Exp. Med. **191**:1581–1590.

5. **Aerts-Toegaert C, Heirman C, Tuyaerts S, Corthals J, Aerts JL, Bonehill A, Thielemans K, Breckpot K.** 2007. CD83 expression on dendritic cells and T cells: correlation with effective immune responses. Eur. J. Immunol. **37**:686–695.

6. **Prechtel AT, Turza NM, Theodoridis AA, Steinkasserer A.** 2007. CD83 knockdown in monocyte-derived dendritic cells by small interfering RNA leads to a diminished T cell stimulation. J. Immunol. **178**:5454–5464.

7. **Prazma CM, Yazawa N, Fujimoto Y, Fujimoto M, Tedder TF.** 2007. CD83 expression is a sensitive marker of activation required for B cell and CD4+ T cell longevity in vivo. J. Immunol. **179**:4550–4562.

8. **Lechmann M, Krooshoop DJ, Dudziak D, Kremmer E, Kuhnt C, Figdor CG, Schuler G, Steinkasserer A.** 2001. The extracellular domain of CD83 inhibits dendritic cell-mediated T cell stimulation and binds to a ligand on dendritic cells. J. Exp. Med. **194**:1813–1821.

9. **Scholler N, Hayden-Ledbetter M, Dahlin A, Hellstrom I, Hellstrom KE, Ledbetter JA.** 2002. CD83 regulates the development of cellular immunity. J. Immunol. **168**:2599–2602.

10. **Zinser E, Lechmann M, Golka A, Lutz MB, Steinkasserer A.** 2004. Prevention and treatment of experimental autoimmune encephalomyelitis by soluble CD83. J. Exp. Med. **200**:345–351.

11. **Ge W, Arp J, Lian D, Liu W, Baroja ML, Jiang J, Ramcharran S, Eldeen FZ, Zinser E, Steinkasserer A, Chou P, Brand S, Nicolette C, Garcia B, Wang H.** 2010. Immunosuppression involving soluble CD83 induces tolerogenic dendritic cells that prevent cardiac allograft rejection. Transplantation **90**:1145–1156.

12. **Lan Z, Lian D, Liu W, Arp J, Charlton B, Ge W, Brand S, Healey D, DeBenedette M, Nicolette C, Garcia B, Wang H.** 2010. Prevention of chronic renal allograft rejection by soluble CD83. Transplantation **90**:1278–1285.

13. **Berchtold S, Muhl-Zurbes P, Maczek E, Golka A, Schuler G, Steinkasserer A.** 2002. Cloning and characterization of the promoter region of the human CD83 gene. Immunobiology **205**:231–246.

14. **Maston GA, Evans SK, Green MR.** 2006. Transcriptional regulatory elements in the human genome. Annu. Rev. Genomics Hum. Genet. **7**:29–59.

15. **Lefstin JA, Yamamoto KR.** 1998. Allosteric effects of DNA on transcriptional regulators. Nature **392**:885–888.

16. **Remenyi A, Scholer HR, Wilmanns M.** 2004. Combinatorial control of gene expression. Nat. Struct. Mol. Biol. **11**:812–815.

17. **Cohen CD, Klingenhoff A, Boucherot A, Nitsche A, Henger A, Brunner B, Schmid H, Merkle M, Saleem MA, Koller KP, Werner T, Grone HJ, Nelson PJ, Kretzler M.** 2006. Comparative promoter analysis allows de novo identification of specialized cell junction-associated proteins. Proc. Natl. Acad. Sci. U. S. A. **103**:5682–5687.

18. **Knippertz I, Hesse A, Schunder T, Kampgen E, Brenner MK, Schuler G, Steinkasserer A, Nettelbeck DM.** 2009. Generation of human dendritic cells that simultaneously secrete IL-12 and have migratory capacity by adenoviral gene transfer of hCD40L in combination with IFN-gamma. J. Immunother. **32**:524–538.

19. **Schaft N, Dorrie J, Muller I, Beck V, Baumann S, Schunder T, Kampgen E, Schuler G.** 2006. A new way to generate cytolytic tumor-specific T cells: electroporation of RNA coding for a T cell receptor into T lymphocytes. Cancer Immunol. Immunother. **55**:1132–1141.

20. **Rohmer S, Mainka A, Knippertz I, Hesse A, Nettelbeck DM.** 2008. Insulated hsp70B′ promoter: stringent heat-inducible activity in replication-deficient, but not replication-competent adenoviruses. J. Gene Med. **10**:340–354.

21. **Naschberger E, Werner T, Vicente AB, Guenzi E, Topolt K, Leubert R, Lubeseder-Martellato C, Nelson PJ, Sturzl M.** 2004. Nuclear factor-kappaB motif and interferon-alpha-stimulated response element cooperate in the activation of guanylate-binding protein-1 expression by inflammatory cytokines in endothelial cells. Biochem. J. **379**:409–420.

22. **Milne TA, Zhao K, Hess JL.** 2009. Chromatin immunoprecipitation (ChIP) for analysis of histone modifications and chromatin-associated proteins. Methods Mol. Biol. **538**:409–423.

23. **McCurdy RD, McGrath JJ, Mackay-Sim A.** 2008. Validation of the comparative quantification method of real-time PCR analysis and a cautionary tale of housekeeping gene selection. Gene Ther. Mol. Biol. **12**:15–24.

24. **Pfaffl MW, Tichopad A, Prgomet C, Neuvians TP.** 2004. Determination of stable housekeeping genes, differentially regulated target genes and sample integrity: BestKeeper-Excel-based tool using pair-wise correlations. Biotechnol. Lett. **26**:509–515.

25. **Nencioni A, Beck J, Werth D, Grunebach F, Patrone F, Ballestrero A, Brossart P.** 2007. Histone deacetylase inhibitors affect dendritic cell differentiation and immunogenicity. Clin. Cancer Res. **13**:3933–3941.

26. **Tamura T, Yanai H, Savitsky D, Taniguchi T.** 2008. The IRF family transcription factors in immunity and oncogenesis. Annu. Rev. Immunol. **26**:535–584.

27. **Bros M, Ross XL, Pautz A, Reske-Kunz AB, Ross R.** 2003. The human fascin gene promoter is highly active in mature dendritic cells due to a stage-specific enhancer. J. Immunol. **171**:1825–1834.

28. **Mosialos G, Yamashiro S, Baughman RW, Matsudaira P, Vara L, Matsumura F, Kieff E, Birkenbach M.** 1994. Epstein-Barr virus infection induces expression in B lymphocytes of a novel gene encoding an evolutionarily conserved 55-kilodalton actin-bundling protein. J. Virol. **68**:7320–7328.

29. **Pinkus GS, Pinkus JL, Langhoff E, Matsumura F, Yamashiro S, Mosialos G, Said JW.** 1997. Fascin, a sensitive new marker for Reed-Sternberg cells of Hodgkin's disease. Evidence for a dendritic or B cell derivation? Am. J. Pathol. **150**:543–562.

30. **Hashimoto Y, Skacel M, Adams JC.** 2005. Roles of fascin in human carcinoma motility and signaling: prospects for a novel biomarker? Int. J. Biochem. Cell Biol. **37**:1787–1804.

31. **Hashimoto Y, Loftis DW, Adams JC.** 2009. Fascin-1 promoter activity is regulated by CREB and the aryl hydrocarbon receptor in human carcinoma cells. PLoS One **4**:e5130. doi:10.1371/journal.pone.0005130.

32. **Kawai T, Akira S.** 2006. TLR signaling. Cell Death Differ. **13**:816–825.

33. **Krausgruber T, Saliba D, Ryzhakov G, Lanfrancotti A, Blazek K, Udalova IA.** 2010. IRF5 is required for late-phase TNF secretion by human dendritic cells. Blood **115**:4421–4430.

34. **McKinsey TA, Chu Z, Tedder TF, Ballard DW.** 2000. Transcription factor NF-kappaB regulates inducible CD83 gene expression in activated T lymphocytes. Mol. Immunol. **37**:783–788.

35. **Barnes BJ, Kellum MJ, Field AE, Pitha PM.** 2002. Multiple regulatory domains of IRF-5 control activation, cellular localization, and induction of chemokines that mediate recruitment of T lymphocytes. Mol. Cell. Biol. **22**:5721–5740.

36. **Mancl ME, Hu G, Sangster-Guity N, Olshalsky SL, Hoops K, Fitzgerald-Bocarsly P, Pitha PM, Pinder K, Barnes BJ.** 2005. Two discrete promoters regulate the alternatively spliced human interferon regulatory factor-5

isoforms. Multiple isoforms with distinct cell type-specific expression, localization, regulation, and function. J. Biol. Chem. **280**:21078–21090.

37. **Takaoka A, Yanai H, Kondo S, Duncan G, Negishi H, Mizutani T, Kano S, Honda K, Ohba Y, Mak TW, Taniguchi T.** 2005. Integral role of IRF-5 in the gene induction programme activated by Toll-like receptors. Nature **434**:243–249.

38. **Krausgruber T, Blazek K, Smallie T, Alzabin S, Lockstone H, Sahgal N, Hussell T, Feldmann M, Udalova IA.** 2011. IRF5 promotes inflammatory macrophage polarization and TH1-TH17 responses. Nat. Immunol. **12**: 231–238.

39. **Battistini A.** 2009. Interferon regulatory factors in hematopoietic cell differentiation and immune regulation. J. Interferon Cytokine Res. **29**: 765–780.

40. **Huang B, Qi ZT, Xu Z, Nie P.** 2010. Global characterization of interferon regulatory factor (IRF) genes in vertebrates: glimpse of the diversification in evolution. BMC Immunol. **11**:22. doi:10.1186/1471-2172-11-22.

41. **Tailor P, Tamura T, Ozato K.** 2006. IRF family proteins and type I interferon induction in dendritic cells. Cell Res. **16**:134–140.

42. **Harada H, Fujita T, Miyamoto M, Kimura Y, Maruyama M, Furia A, Miyata T, Taniguchi T.** 1989. Structurally similar but functionally distinct factors, IRF-1 and IRF-2, bind to the same regulatory elements of IFN and IFN-inducible genes. Cell **58**:729–739.

43. **Taniguchi T.** 1995. IRF-1 and IRF-2 as regulators of the interferon system and cell growth. Indian J. Biochem. Biophys. **32**:235–239.

44. **Taniguchi T, Ogasawara K, Takaoka A, Tanaka N.** 2001. IRF family of transcription factors as regulators of host defense. Annu. Rev. Immunol. **19**:623–655.

45. **Masumi A.** 2011. Histone acetyltransferases as regulators of nonhistone proteins: the role of interferon regulatory factor acetylation on gene transcription. J. Biomed. Biotechnol. **2011**:640610. doi:10.1155/2011/640610.

46. **Masumi A, Ozato K.** 2001. Coactivator p300 acetylates the interferon regulatory factor-2 in U937 cells following phorbol ester treatment. J. Biol. Chem. **276**:20973–20980.

47. **Marsili G, Remoli AL, Sgarbanti M, Battistini A.** 2004. Role of acetylases and deacetylase inhibitors in IRF-1-mediated HIV-1 long terminal repeat transcription. Ann. N. Y. Acad. Sci. **1030**:636–643.

48. **Cartharius K, Frech K, Grote K, Klocke B, Haltmeier M, Klingenhoff A, Frisch M, Bayerlein M, Werner T.** 2005. MatInspector and beyond: promoter analysis based on transcription factor binding sites. Bioinformatics **21**:2933–2942.

49. **Ouyang X, Negishi H, Takeda R, Fujita Y, Taniguchi T, Honda K.** 2007. Cooperation between MyD88 and TRIF pathways in TLR synergy via IRF5 activation. Biochem. Biophys. Res. Commun. **354**:1045–1051.

50. **Cope NF, Fraser P, Eskiw CH.** 2010. The yin and yang of chromatin spatial organization. Genome Biol. **11**:204. doi:10.1186/gb-2010-11-3-204.

51. **Saiz L, Vilar JM.** 2006. DNA looping: the consequences and its control. Curr. Opin. Struct. Biol. **16**:344–350.

52. **Johnson S, Linden M, Phillips R.** 2012. Sequence dependence of transcription factor-mediated DNA looping. Nucleic Acids Res. **40**:7728–7738.

53. **Werner T.** 2010. Next generation sequencing in functional genomics. Brief. Bioinform. **11**:499–511.

54. **Johnson DR, Pober JS.** 1994. HLA class I heavy-chain gene promoter elements mediating synergy between tumor necrosis factor and interferons. Mol. Cell. Biol. **14**:1322–1332.

55. **Ohmori Y, Hamilton TA.** 1995. The interferon-stimulated response element and a kappa B site mediate synergistic induction of murine IP-10 gene transcription by IFN-gamma and TNF-alpha. J. Immunol. **154**: 5235–5244.